An assessment of summer sensible heat flux on the Tibetan Plateau from eight data sets

ZHU XiaYing[1,2], LIU YiMin[1*] & WU GuoXiong[1]

[1] *State Key Laboratory of Numerical Modeling for Atmospheric Sciences and Geophysical Fluid Dynamics (LASG), Institute of Atmospheric Physics, Chinese Academy of Sciences, Beijing 100029, China;*
[2] *National Climate Center, China Meteorological Administration, Beijing 100081, China*

The eight datasets of the summer (June–August) surface sensible heat (SH) flux over the Tibetan Plateau (TP) are compared on the time scales of the climatology, interannual variability and linear trend during 1980–2006. These data sets include five reanalyses (National Center for Environmental Prediction reanalysis, NCEPR1 and NCEPR2, NCEP climate forecast system reanalysis, CFSR, Japanese 25-year reanalysis, JRA, and European Centre for Medium Range Weather Forecasts reanalysis, ERA40), two land surface model outputs (Noah model data of Global Land Data Assimilation System version 2, G2_Noah, and Simple Biosphere version 2 output by Yang et al., YSiB2), and estimated SH based on China Meteorological Administration (CMA) station observations, ObCh. The results suggest that the summer SH on the TP differs from one dataset to another due to different inputs and calculations. Climatologically, the ERA40 and JRA distribute rather uniformly while the other six products show similar regional disparities, that is, larger in the west than in the east and stronger in the north and the south than in the middle of the plateau. The mean magnitude of the SH averaged over the 76 stations above the TP varies considerably among each dataset with the difference of more than 20 W m^{-2} between the maximum (G2_Noah) and minimum (ObCh). Nevertheless, they are consistent in the interannual variability and mostly show a significant decreasing trend corresponding to the weakening surface wind speed, in spite of the distinct trend for the ground-air temperature difference among the different data sets. These two consistencies indicate the particular availability of the SH products, which is helpful to the relevant climate dynamics research.

Tibetan Plateau, sensible heat flux assessment, interannual variation, linear trend

The uplifted Tibetan Plateau (TP) in summer provides powerful sensible heating to the atmosphere that causes its intersection with the lower-layer isentropic surfaces, producing low-level cyclonic and high-level anti-cyclonic circulation [1, 2]. Since many previous studies showed that sensible heating of the TP exerts a crucial impact on atmospheric circulation in the Asian summer monsoon region [3–7], it is necessary to investigate the spatiotemporal characteristics of the TP surface sensible heat (SH) flux. However, there are few directly observed SH data of large scale and long time in the world, not to mention for the TP covered with complex terrain and relatively few meteorological sites. Thus the estimation of the TP SH is always in dispute.

The bulk aerodynamic method is typically used to estimate SH flux, when how to determine the heat transfer coefficient (C_H) becomes a crux. Considering the form drag in mountain regions, Cressman [8] suggested the surface momentum transfer coefficient ranging over 0.005–0.009, in light of which Ye et al. [9] selected 0.008. Using data ob-

---

tained by the First Qinghai-Xizang (Tibet) Plateau Meteorological Experiment (TIPMEX), Chen and Wong [10] derived a parameterization scheme for a 10-day mean C_H (hereafter called the Chen-Wong scheme) from the surface energy budget. In this scheme SH is inversely proportional to wind speed, excluding the impact of atmospheric stability. Given the average wind speed during the TIPMEX, Chen et al. [11] adopted this scheme to estimate the average of C_H as 0.0036 (hereafter called the Chen scheme). In addition, Zhang et al. [12] obtained the mean C_H about 0.004–0.005 using similar data. Taking into account the effect of both the atmospheric stability and thermal roughness length, Yang et al. [13] proposed a new parameterization scheme (referred to as Yang scheme) based on micrometeorological theory. Employing the China Meteorological Administration (CMA) station observations, Yang et al. [14] compared the above mentioned three different schemes, and concluded that the climate SH on the TP was greater by Yang scheme than by the other two; the annual SH from Chen or Yang schemes decreased during 1984–2006 by contrast with the weakly increasing trend of that by Chen-Wong scheme. Therefore, the estimated SH over the TP would be in great diversity due to different parameters and parameterization schemes in spite of the same input fields.

Station observations are one of the bases for diagnosis, but still there are several defects that are not negligible, such as a small number of sites scattered unevenly on the TP. Therefore, reanalysis data or model outputs without those defects are much more popular. But to what extent are they different from the station observations? For the multi-year average, the TP temperature and heat flux provided by the National Centers for Environmental Prediction (NCEP) reanalysis-I (NCEPR1) [15] and II (NCEPR2) [16] have seasonal changes close to the actual, but the values of temperature are systematically smaller mainly due to the discrepancy of terrain height between model grids and stations [17, 18]. In terms of climate change on the TP during 1958–2000, the surface temperature from either the NCEPR1 or the European Centre for Medium Range Weather Forecasts (ECMWF) 45-year reanalysis (ERA40) [19] has no obvious trend,   not conforming to the warming station observations [20, 21]. The above investigations mainly concerned the reliability of temperature and relatively few studies examined the SH, and thus it is necessary to assess it from the existing various datasets with the emergence of new data. This paper introduces a variety of SH data with a long time scale, and then compares their method of calculation, and finally investigates the climate mean, interannual variation and linear trend of the summer SH from 1980 to 2006.

1   Data

In this paper eight datasets are used, including five reanalyses, two land surface model outputs and estimated SH based on station observations utilizing Chen scheme. Five reanalysis data are NCEPR1, NCEPR2, NCEP Climate Forecast System Reanalysis (CFSR) [22], ERA40, and the Japanese 25-year Reanalysis (JRA) [23]. Their horizontal resolution is classified into two types, T62 Gaussian (192×94 grid points) for the first three datasets and T106 Gaussian (320×160 grid points) for the latter two. In all datasets SH is a cumulative average within six hours, so are the surface skin temperature and 2 m air temperature in the CFSR and JRA, while these two variables in the rest reanalyses are the instantaneous average of four times a day, the same as near-surface wind speed. In addition, the ERA40 near-surface wind speed is in the resolution of 2.5° latitude by 2.5° longitude grid instead of T62 Gaussian, since the latter is not available and the monthly meridional and zonal wind components of the high and low resolution are equivalent (figures not shown) for the plateau (25°–40°N, 80°–102.5°E).

The above five reanalyses have both strengths and weaknesses. The NCEPR1 and ERA40 span much longer time, especially the NCEPR1 starting in 1948 and continuing to this day but having many human errors. However, the NCEPR2, with a shorter time period from 1979 to present, corrected these errors, simply assimilated the Climate Prediction Center (CPC) Merged Analysis of Precipitation (CMAP), modified some of the physical processes and parameterization schemes in the model, and improved simulations of soil moisture, surface temperature, and radiation [16]. The ERA40 used an improved 3-dimensional assimilation system and assimilated more satellite and station observations such as surface moisture and snow depth [19]. The JRA assimilated the observations similar to those of the ERA40, except that it also used the snow data in China [23]. The CFSR is a high-resolution sea-land-air-ice coupling global reanalysis, utilizing semi-coupled global land data assimilation system (GLDAS) with Noah land surface model [24] and the land information System (LIS) from United States National Aeronautics and Space Administration (NASA) [25]. Its atmospheric forcing fields are the CFSR atmospheric assimilation outputs and observed precipitation. CFSR GLDAS/LIS adopted observed global precipitation analyses as direct forcing to the land surface analysis, rather than the typical analysis approach of using precipitation from the assimilating background atmospheric patterns (NCEPR1) or using observed precipitation to "nudge" soil moisture (NCEPR2). The blending function of precipitation is latitude dependent, favoring the satellite-based CMAP analysis in the tropics, the gauge analysis in the mid-latitudes, and the model precipitation in high latitudes. Overall, the primary novelties of the CFSR are (1) the coupling to the ocean during the generation of the 6-h guess field, (2) the high resolution, and (3) the grid statistical interpolation of the satellite radiances rather than the derived temperature and moisture for the entire period.

One of the two land surface model outputs is provided by the Noah land surface model of NASA GLDAS version 2 (referred to as the G2_Noah, horizontal resolution of 1° latitude by 1° longitude grid, the time interval of 3 h) [26] and the other is by Yang et al. [27, 28] via the simple biosphere model (SiB2) [29], hereafter called the YSiB2. Using state fields from the LSM climatology for that day of the year, G2_Noah was forced by the global meteorological forcing datasets from Princeton University [30], while the GLDAS version 1 was forced by several data sources in different period, leading to some of the fields discontinuous from year to year. Input fields of the YSiB2 are the CMA station observations downscaled to half an hour in the light of the application premise of Monin-Obukhov similarity theory [31], which demands that the air flow must be uniform and approximately steady. Additionally, the YSiB2 was obtained through the improved SiB2 model adjusting to the TP surface conditions based on the TP experiments.

Based on the CMA station observations four times a day via Chen scheme (C_H=0.004), the SH flux over the TP was calculated (hereafter called the ObCh), in which the atmospheric density was the monthly climatology derived by the ideal gas law. Seventy-six stations with fewer missing data on the TP were selected in the YSiB2 and ObCh. Besides the daily maximum wind speed, the YSiB2 made use of the 6-h near-surface wind speed, the same as the ObCh, which was used for both two data in the following comparison so that the wind speed was identical between the ObCh and YSiB2.

If not specified, the data here are all for June-August during the period of 1980–2006 except the ERA40, which is from 1980 to 2001.

2   Calculation method of the SH

The SH fluxes from the eight data are all calculated via the bulk aerodynamic method, that is,

$$H = \rho c_p C_H V (T_s - T_a), \qquad (1)$$

where H is the SH, ρ is air density, c_p is the specific heat at a constant pressure, V is wind speed at 10 m, T_s is surface skin temperature, T_a is air temperature at 2 m, and C_H is bulk heat transfer coefficient. This equation is one of the most important applications of the Monin-Obukhov similarity theory. By this formula SH could be directly derived given C_H which, however, is experiential and usually decided through parameterization.

Parameterizations of heat transfer coefficient can be classified mainly into two types [32]. One is a simple explicit formula of the bulk Richardson number [33], such as the NCEPR1 and R2 [34, 35] and JRA [36]. This scheme has the advantage of faster computation at the expense of accuracy. The other is an implicit function of the Obukhov

length [37], such as the ERA40 [38], CFSR and G2_Noah [32], and YSiB2 [39]. Although this scheme, in which the roughness length for momentum, heat and humidity is independent, is more expensive in calculation, it is easier to modify its stability functions should more accurate and/or extensive field observations in the future motivate refinements to the stability functions.

Since these land surface parameterization schemes are all based on the Monin-Obukhov similarity theory, the different selection of these schemes does not result in significant changes in surface fluxes, skin temperature, and precipitation, given the same treatment of roughness length for heat and the same input data, while the thermal roughness length would take a crucial effect [32]. To retrieve the roughness length for heat, the CFSR and G2_Noah employed the Zilitinkevich equation [40], which could improve the surface heat flux and skin temperature simulations proved by the sensitivity test of one dimensional column model, and also could reduce forecast precipitation bias indicated by the long-term test of the NCEP mesoscale Eta forecast model [32]. However, Yang et al. [41] pointed out that the Zilitinkevich equation overestimated daytime thermal roughness length on the TP, which had an obvious diurnal cycle of small in the day and large at night, and thus overmeasured the sensible heat flux and underestimated the ground temperature. It was also suggested that the diurnal variation of thermal roughness length could be better simulated using the friction velocity along with friction temperature [39].

Notably, both the force fields and parameterization schemes of these datasets are different, so we cannot determine which parameterization scheme of C_H is better and also there is no adequate information about this coefficient. Besides, how the real C_H varies inter-annually and at longer time-scale is a challenge at present due to the lack of adequate observations. Therefore, quantifying the difference in the thermal transfer coefficient is beyond the scope of this paper, which will focus on the climate mean, inter-annual change and linear trend of summer SH over the TP as well as the relationship with the surface wind speed and ground-air temperature contrast. This provides a reference for future research on the TP thermal forcing and model simulations.

3   Result

3.1   Climatology of summer mean

As mentioned previously, differences of either calculations or input fields may lead to huge differences in SH flux as it is estimated by the bulk formula in this paper. The climatology of summer SH on the TP (Figure 1) shows its spatial pattern of greater in the west as well as north and south flanks than in the east as well as the middle of the plateau in most data except for ERA40 and JRA, which agrees with
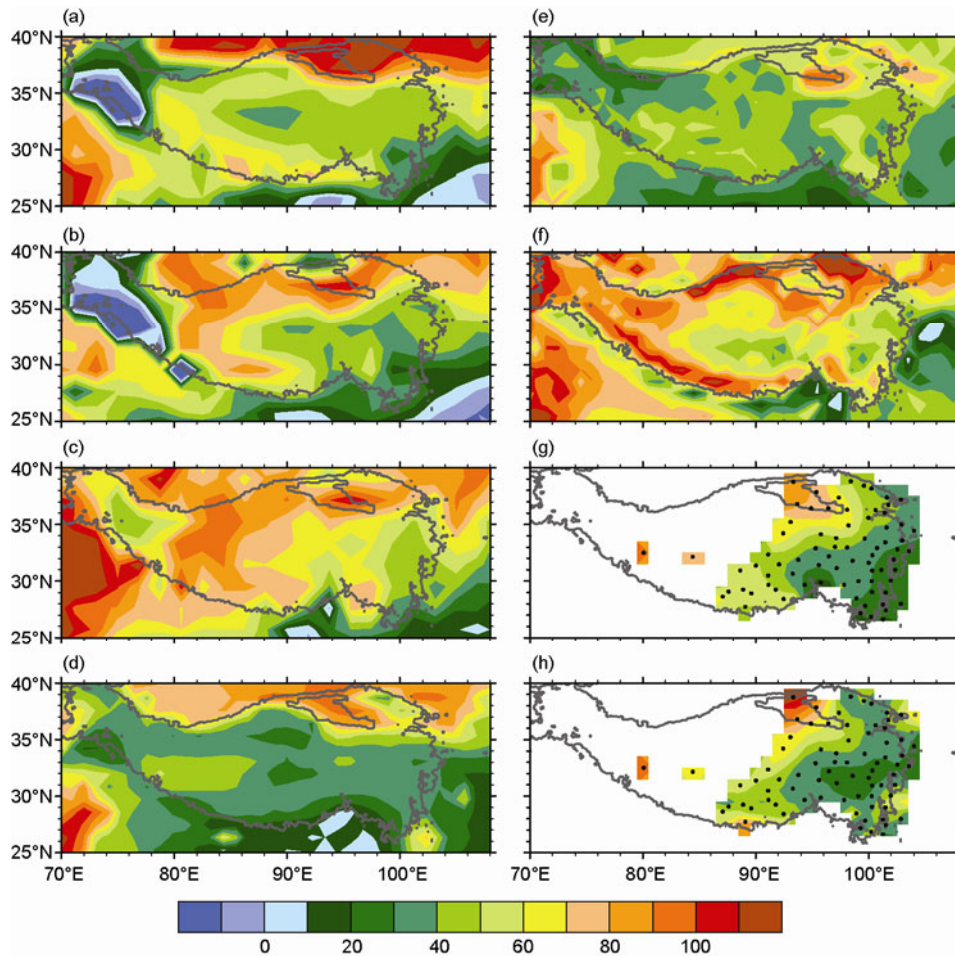
Figure 1 Spatial distribution of the climatology of summer (June–August) sensible heat flux on the Tibetan Plateau from eight sources (W m^{-2}). (a) NCEPR1; (b) NCEPR2; (c) CFSR; (d) ERA40; (e) JRA; (f) G2_Noah; (g) YSiB2; (h) ObCh. The gray line stands for 3000 m height and dark circles for stations.

the ground-air temperature difference. The SH spreads quite uniformly and the value is generally smaller for ERA40 and JRA, which assimilate similar observations. Also both of them use 2D optimal interpolation, which does not allow information from the upper atmosphere to impact the surface analysis, instead of 3D variational assimilation method to derive the near surface atmospheric forcing variables [23, 42]. Different from the other products, the NCEPR1 and R2 have notable negative SH values in Kashmir region. That may be caused by snow cover that makes the skin temperature lower than air temperature in the model.

In the remainder of this paper we will focus on the situation in the central and eastern TP where much more meteorology sites covered. Figure 1 suggests that the SH fluxes from YSiB2 and ObCh are equivalent, probably because these two reanalyses were forced by almost the same CMA station observations, except that in YSiB2 six-hourly data were downscaled to half an hour. Accordingly the YSiB2 took into account the diurnal variation of thermal transfer coefficient, thus in theory it should be closer to the real, which, however, there have been few observed half-hourly

SH to verify. Nevertheless, the equivalent values derived from these two data do indicate the particular applicability of Chen scheme. Compared with the NCEPR1, NCEPR2 is closer to YSiB2 and ObCh in the SH spatial distribution. It is known that NCEPR2 has corrected some mandatory errors found in NCEPR1, such as snow data during 1974–1994 and false skin temperature when there is no wind [16]. Although the CFSR and G2_Noah both employed Noah land surface model, they are apparently different from each other in SH, which is probably related to the different atmospheric forcing fields. Within CFSR the semi-coupled GLDAS is forced with the CFSR atmospheric data assimilation output and observed precipitation, whereas in G2_Noah as a pure land surface model the atmospheric forcing fields are given.

The above analysis shows that the summer SH on the TP is distributed variously from one data to another climatologically due to the different forcing fields and model such as its resolution, assimilation and parameterization. Then what about their inter-annual and longer-term change?

3.2   Interannual and long-term change

To quantitatively compare the temporal variation of eight datasets, grid data were interpolated to 76 stations the same as ObCh via bilinear interpolation. Figure 2(a) depicts the SH averaged by 76 sites on the TP from year to year. Apparently, they are of great difference among each other. Generally, the G2_Noah is the strongest with the climatology up to 64 W m^{-2} (Table 1), followed by the CFSR, while the ERA40, YSiB2, and ObCh are the weakest with an average of about 42 W m^{-2}. This is consistent with the horizontal distribution of SH in Figure 1. As far as their interannual variation magnitude is concerned, the CFSR, which has a sharp rise during 1980–1986, is the greatest with the standard deviation (SD) of about 6 W m^{-2}, while the YSiB2 is the weakest with SD of about 3 W m^{-2}, only half that of CFSR.

Although the SH has various inter-annual fluctuations among the eight datasets, the correlation between ObCh and the others all exceeds the 95% confidence level of *t*-test (Table 1). The correlation coefficient with YSiB2 is the highest, of which above 0.8 is possibly attributed to the use of CMA observation. Among the five reanalyses, ERA40 and JRA are better correlated with ObCh, and the CFSR is worse correlated due to the sharp rise during 1980–1986. Correlations of the NCEPR1 and NCEPR2 with ObCh become significant without the linear trends.

As for the long term trend, SH from CFSR was much less in 1980 and 1981 than the other years so that it increased rapidly in the early 1980s but followed by a downward trend. All the other data show a linear trend of weakening, in which the G2_Noah decreased most steeply, about 4 W m^{-2} decade^{-1}, while YSiB2 weakened least, under 2 W m^{-2} decade^{-1}, and JRA and ObCh were similar with the weakening trend of 2–3 W m^{-2} decade^{-1}. It can be concluded that the TP SH for summer has been decreasing since the mid-1980s showed by all the eight datasets.
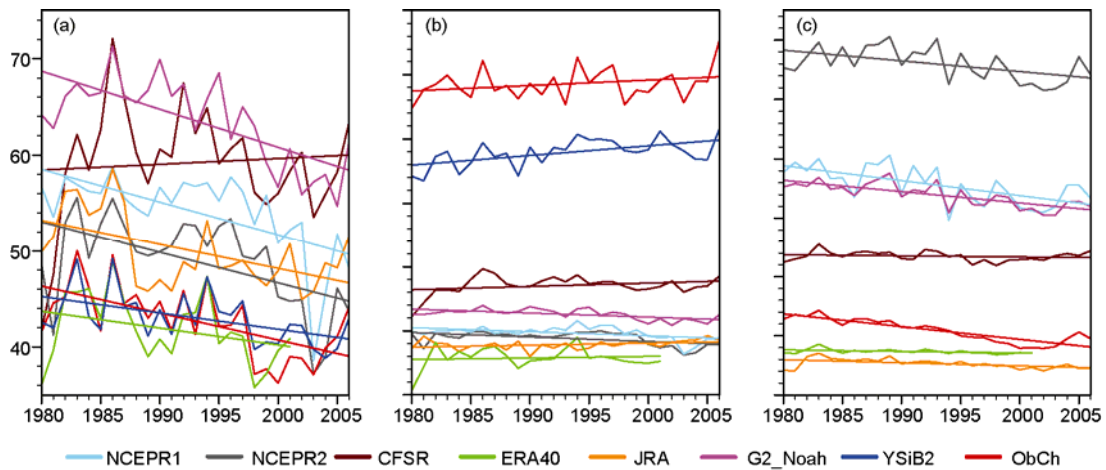

Figure 2   The interannual variation and linear trends of the summer (a) the sensible heat flux (in W m^{-2}), (b) ground-air temperature difference (K), and (c) wind speed at 10 m (m s^{-1}) averaged by 76 stations on the Tibetan Plateau.

Table 1   The climatology, standard deviation (SD), and linear trend (every 10 years) of the summer sensible heat (SH), ground-air temperature difference T_s–T_a, and surface wind speed V averaged by 76 stations on the Tibetan Plateau and the interannual correlation with the corresponding variables from ObCh[a)]

		NCEPR1	NCEPR2	CFSR	ERA40	JRA	G2_Noah	YSiB2	ObCh
SH (W m^{-2})	Climatology	54.10	48.91	59.24	41.87	49.95	63.58	43.02	42.68
	SD	4.33	4.75	5.88	3.54	3.78	4.39	2.68	3.65
	Trend	**−3.40**	**−3.20**	0.60	−1.75	**−2.51**	**−3.95**	**−1.70**	**−2.81**
	Correlation coefficient	**0.56** (0.28)	**0.55** (0.33)	**0.49** **(0.68)**	**0.77** **(0.75)**	**0.66** **(0.51)**	**0.74** **(0.55)**	**0.87** **(0.83)**	1 1
T_s–T_a (K)	Climatology	0.97	0.88	1.71	0.58	0.79	1.26	3.79	4.86
	SD	0.11	0.11	0.15	0.16	0.07	0.08	0.21	0.24
	Trend	**−0.06**	**−0.07**	0.05	0.03	0.03	**−0.06**	0.15	0.08
	Correlation coefficient	0.26 **(0.46)**	0.02 (0.20)	**0.54** **(0.50)**	**0.51** **(0.50)**	−0.04 (−0.15)	0.15 **(0.43)**	**0.65** **(0.62)**	1 1
V (m s^{-1})	Climatology	4.56	6.60	3.35	1.73	1.53	4.39	2.09	2.09
	SD	0.31	0.27	0.08	0.04	0.08	0.20	0.19	0.19
	Trend	**−0.25**	**−0.18**	−0.02	**−0.03**	**−0.05**	**−0.19**	**−0.22**	**−0.22**
	Correlation coefficient	**0.75** **(0.51)**	**0.65** **(0.48)**	**0.48** **(0.69)**	**0.59** **(0.50)**	**0.62** **(0.41)**	**0.81** **(0.47)**	1 1	1 1

a) Bold figures exceed the 95% confidence level of *t*-test. Figures in brackets are correlation coefficient of variables without the linear trend.

Since surface wind speed and ground-air temperature contrast are two of the key elements for SH estimation, this paper also analyzed the interannual and long-term change of them over the plateau (Figure 2(b), (c)). In general, ground-air temperature difference from all the eight datasets is positive, indicating that the surface skin is warmer than air over the plateau for summer mean. But there exist significant differences between various types of data. The ObCh has the largest temperature difference of about 5 K, followed by YSiB2 about 4 K, while the other six datasets are less than 2 K and ERA40 is the smallest about 0.6 K. Although the surface-air temperature difference varies from one dataset to another, it is significantly correlated between the station observation and YSiB2, ERA40 as well as CFSR with the coefficients of above 0.5. From the viewpoint of long time change, the YSiB2 shows a significant increasing trend, whereas G2_Noah, NCEPR1 and NCEPR2 perform a prominent decreasing trend, and the other four kinds of datasets have no distinct trend (Table 1).

Though the reanalysis data assimilated observed surface wind, impact of the differences in model on surface wind speed could not be neglected [15]. As shown in Figure 2(c), the wind speed curve is different obviously among various datasets. The NCEPR2 is maximum up to 6.6 m s^{-1}, and JRA is minimum with an average of 1.5 m s^{-1}. Compared to the station observations of YSiB2 and ObCh which are about 2 m s^{-1}, the JRA and ERA40 are slightly weaker, while the CFSR, G2_Noah, NCEPR1 and NCEPR2 are notably stronger. In spite of these differences, they are significantly correlated with station observations interannually, indicating that the wind speed is quite consistent in the interannual variation among these datasets though the magnitude of temporal change is diverse, for example, the fluctuation is the largest for NCEPR1 and NCEPR2 by contrast to ERA40, which is the smallest. Besides the coherence of its interannual variability, the wind speed has significant weakening linear tendency except for the CFSR with a weak linear trend. The NCEPR1 and station observed wind speed reduces most strongly about 0.2 m s^{-1} decade^{-1}.

3.3   Internal consistency within each dataset

SH flux, possessing a notable diurnal cycle, is a nonlinear term. Hence, it may lead to large bias to calculate SH simply using the daily mean of wind speed and ground-air temperature difference, which also have strong diurnal change.

The curves of these three variables (Figure 2) show that all of them are smaller from ERA40 with respect to the other datasets. However, the SH from JRA is much stronger though the other two variables are close to the ERA40, indicating that the transient part in SH may have an important contribution for this reanalysis. Although the ObCh (NCEPR2) is the largest in ground-air temperature difference (wind speed), its SH is relatively small along with the weaker wind speed (ground-air temperature difference). This suggests that the SH values depend on different factors within each dataset, so does its temporal change (Table 2). The SH flux along with wind speed has a significant decreasing trend from all the eight datasets except for CFSR, though the linear trends of ground-air temperature difference are diverse among each dataset. Without the linear trend, the SH is correlated significantly with ground-air temperature difference, while its correlation with wind speed is fairly poor within all the eight datasets except for JRA. All in all, the relationship between SH and wind speed as well as ground-air temperature contrast is considerably different given different datasets, which may be attributed to the inconsistent description of meteorological fields in diurnal changes.

4   Discussion and conclusion

Comparisons of eight datasets in the SH and related variables in this paper clearly show great differences in the climate mean and interannual variation as well as long-term change of the SH provided by each dataset due to the disparities of force fields and parameterization schemes.

For the climatology of summer SH, most data have the feature of stronger in the west than in the east of TP, which is consistent with previous studies [14, 43]. This is because in summer on the plateau it is wetter and has more rain in the east while it is drier in the west without much rain [44]. It is also found that SH in the north and south sides is larger with respect to that in the mid-region, which is likely to be associated with the vegetation types [26]. The ground is almost bare in northern plateau where evaporation and heat roughness are very small, responsible for large ground-air temperature difference and strong SH flux. Nevertheless with respect to the middle and east TP covered with dense bush, the narrow band highland above 3000 m in the south TP scattered with sparse shrub has a smaller thermal

Table 2   Correlation coefficients of the TP SH in summer and ground-air temperature difference (r_t) as well as surface wind speed (r_v) within each dataset[a]

	NCEPR1	NCEPR2	CFSR	ERA40	JRA	G2_Noah	YSiB2	ObCh
r_t	**0.93**	**0.92**	**0.94**	**0.77**	−0.09	**0.96**	0.31	**0.49**
	(0.92)	(0.89)	(0.96)	(0.85)	(0.12)	(0.95)	(0.84)	(0.87)
r_v	0.26	**0.64**	0.47	0.50	0.45	0.58	0.55	0.78
	(−0.23)	(0.50)	(0.49)	(0.42)	(0.24)	(0.09)	(0.25)	(0.67)

a) Bold figures exceed the 95% confidence level of *t*-test. Figures in brackets are correlation coefficient of variables without the linear trend.

roughness length, which is related to a weaker thermal mixture in boundary layer, and consequently a larger land–air temperature difference and SH. Of all the eight datasets, this spatial characteristic of SH is most prominent from G2_Noah as a pure land surface model. Averaged by 76 stations on the TP, the SH is the strongest from G2_Noah followed by the CFSR, and the ERA40, YSiB2 and ObCh are the weakest. For ERA40, the ground-air temperature difference and wind speed are almost the smallest as well. In contrary, the ObCh has the greatest ground-air temperature difference, which is probably because the station observed ground temperature basically reflects the bare land skin temperature, but in fact the central and eastern plateau is covered with vegetation. This consequently leads to the estimated land-air temperature difference higher than the actual. For YSiB2 using similar observations, the ground temperature is derived from the land surface model, which has taken into account the impact of land surface types, so its ground-air temperature difference is smaller than the station observations [14]. Nonetheless, the ground-air temperature difference from these two sets of station data is significantly greater than the others, either in the central-east covered with vegetation or in the bare east west (figures not shown), indicating that it is too small from the six grid data.

Except NCEPR1 and R2, the other six datasets are consistent in the interannual variation of summer SH over the TP, but the magnitude is quite different; the CFSR is the strongest and YSiB2 the weakest. Compared to ObCh, the other datasets are all well correlated in the SH and surface wind speed and diversely correlated in the land-air temperature difference. This is because in the reanalysis and land surface models, though some of the observations are assimilated, ground temperature is derived from the energy balance, thus more dependent on the parameterizations and input fields. In fact, either the ground temperature or air temperature at 2 m is quite consistent in interannual variability (figures not shown) in spite of discrepancies in the values. However, the interannual change of the difference of these two temperatures is much more differentiated between the model outputs and observational data because of the accumulated errors within each variable.

As far as the linear trend is concerned, the TP averaged surface SH and wind speeds are significantly decreasing from most datasets except for CFSR, while the ground-air temperature difference from each data has various trends, that is, the YSiB2 is significantly increasing inversed to the G2_Noah, NCEPR1 and NCEPR2 decreasing significantly, and that of the remaining four datasets had no significant tendency. This inconsistency is probably associated with their forcing fields and thermodynamic parameterizations. Given the constant radiation and air temperature, the SH flux would reduce along with weakening wind speed while the ground-air temperature difference would increase to maintain the surface energy balance.

The SH is weaker from YSiB2 than from ObCh in not only the magnitude of its linear trend but also that of the interannual variability. This is likely because the heat transfer coefficient of YSiB2 changes with wind speed and ground-air temperature difference, i.e. the smaller the wind speed and the greater the ground-air temperature difference, the more unstable the atmosphere, and hence the greater the heat transfer coefficient [14]. In other words, the heat exchange coefficient for YSiB2 is inversed with wind speed, which weakens the decreasing magnitude of SH caused by weakening wind speed, while the coefficient is fixed for ObCh. Therefore, the temporal change of SH is stronger from ObCh than the YSiB2.

This paper is intended to reveal some of the similarities and differences of summer SH on the TP in its spatial distribution, climate mean, inter-annual change and linear trend among the eight datasets, which provides reference for further research in the impact of TP SH on climate. There are a diversity of causes for the differences, such as the reanalysis scheme, the parameterization of numerical models (especially land surface processes), and forcing fields, which are not fully discussed here due to a lack of adequate data and model introduction and thus needs further investigation.

1   Wu G X, Liu Y M, Liu X, et al. How the heating over the Tibetan Plateau affects the Asian climate in summer (in Chinese). Chin J Atmos Sci, 2005, 29: 47–56

2   Li W P, Wu G X, Liu Y M, et al. How the surface processes over the Tibetan Plateau affect the summertime Tibetan anticyclone-numerical experiments (in Chinese). Chin J Atmos Sci, 2001, 25: 809–816

3   Hu J L, Zhu Q G. Numerical experiments with effects of sensible heating of the Tibetan Plateau on July atmospheric general circulation and summer monsoon in Aisia (in Chinese). J Tropical Meteorol, 1993, 9: 78–84

4   Zhu Q G, Guan Z Y. Numerical study of influence of Tibetan sensible heating abnormality on summer Asian monsoon LFO (in Chinese). J Nanjing Inst Meteorol, 1997, 20: 186–192

5   Duan A M, Liu Y M, Wu G X. Heating status of the Tibetan Plateau from April to June and rainfall and atmospheric circulation anomaly over East Asia in midsummer. Sci China Ser D-Earth Sci, 2003, 48: 250–257

6   Wu G X, Liu X, Zhang Q, et al. Progresses in the study of the climate impacts of the elevated heating over the Tibetan Plateau (in Chinese). Clim Environ Res, 2002, 7: 184–201

7   Zuo Z, Zhang R, Zhao P. The relation of vegetation over the Tibetan Plateau to rainfall in China during the boreal summer. Clim Dyn, 2010, 36: 1207–1219

8   Cressman G P. Improved terrain effects in barotropic forecasts. Mon Weather Rev, 1960, 88: 327–342

9   Ye D Z, Gao Y X, Zhou M Y, et al. The Meteorology of

Qinghai-Xizang (Tibet) Plateau (in Chinese). Beijing: Science Press. 1979. 278

10   Chen W L, Wong D M. A preliminary study on the computational method of 10-day mean sensible heat and latent heat on the Tibetan Plateau. Collected Works of the Qinghai-Xizang Plateau Meteorological Experiment (Series 2) (in Chinese). Beijing: Science Press, 1984. 35–45

11   Chen L, Reiter E R, Feng Z. The atmospheric heat source over the Tibetan Plateau: May–August 1979. Mon Weather Rev, 1985, 113: 1771–1790

12   Zhang J J, Zhu B Z, Zhu F K. Advances in the Qinghai-Xizang Plateau Meteorology—The Qinghai-Xizang Plateau Meteorological Experiment (1979) and Research (in Chinese). Beijing: Science Press, 1988. 268

13   Yang K, Qin J, Guo X, et al. Method development for estimating sensible heat flux over the Tibetan Plateau from CMA data. J Appl Meteorol Climatol, 2009, 48: 2474–2486

14   Yang K, Guo X F, Wu B Y. Recent trends in surface sensible heat flux on the Tibetan Plateau. Sci China Earth Sci, 2010, 54: 19–28

15   Kalnay E, Kanamitsu M, Kistler R, et al. The NCEP/NCAR 40-year reanalysis project. Bull Amer Meteorol Soc, 1996, 77: 437–471

16   Kanamitsu M, Ebisuzaki W, Woollen J, et al. NCEP–DOE AMIP-II Reanalysis (R-2). Bull Amer Meteorol Soc, 2002, 83: 1631–1643

17   Wei L, Li D L. Evaluation of NCEP/DOE surface flux data over Qinghai-Xizang Plateau (in Chinese). Plateau Meteor, 2003, 22: 478–487

18   Su Z X, Lv S H, Luo S W. The examinations and analysis of NCEP/NCAR 40 years global reanalysis data in China (in Chinese). Plateau Meteor, 1999, 18: 209–218

19   Uppala S M, K llberg P W, Simmons A J, et al. The ERA-40 re-analysis. Q J R Meteorol Soc, 2005, 131: 2961–3012

20   Li C, Zhang T J, Chen J. Climatic change of Qinghai-Xizang Plateau region in recent 40-year reanalysis and surface observation data —Contrast of observational data and NCEP, ECMWF surface air temperature and precipitation (in Chinese). Plateau Meteor, 2004, 23(Suppl): 97–103

21   Frauenfeld O W. Climate change and variability using European Centre for Medium-Range Weather Forecasts reanalysis (ERA-40) temperatures on the Tibetan Plateau. J Geophys Res, 2005, 110: D02101

22   Saha S, Moorthi S, Pan H L, et al. The NCEP climate forecast system reanalysis. Bull Amer Meteorol Soc, 2010, 91: 1015–1057

23   Onogi K, Tsutsui J, Koide H, et al. The JRA-25 reanalysis. J Meteorol Soc Jpn, 2007, 85: 369–432

24   Ek M, Mitchell K, Lin Y, et al. Implementation of Noah land surface model advances in the National Centers for Environmental Prediction operational mesoscale Eta model. J Geophys Res, 2003, 108: 8851

25   Peters-Lidard C, Houser P, Tian Y, et al. High-performance Earth system modeling with NASA/GSFC's Land Information System. Inn Syst Software Eng, 2007, 3: 157–165

26   Rodell M, Houser P, Jambor U, et al. The global land data assimilation system. Bull Amer Meteorol Soc, 2004, 85: 381–394

27   Yang K, Guo X, He J, et al. On the climatology and trend of the atmospheric heat source over the Tibetan Plateau: An exper-
iments-supported revisit. J Clim, 2011, 24: 1525–1541

28   Yang K, Chen Y, Qin J. Some practical notes on the land surface modeling in the Tibetan Plateau. Hydrol Earth Syst Sci, 2009, 13: 687–701

29   Sellers P, Randall D, Collatz G, et al. A revised land surface parameterization (SiB2) for atmospheric GCMs. Part I: Model formulation. J Clim, 1996, 9: 676–705

30   Sheffield J, Goteti G, Wood E F. Development of a 50-yr high-resolution global dataset of meteorological forcings for land surface modeling. J Clim, 2006, 19: 3088–3111

31   Monin A, Obukhov A. Basic laws of turbulent mixing in the surface layer of the atmosphere. Tr Akad Nauk SSSR Geophiz Inst, 1954, 24: 163–187

32   Chen F, Janji Z, Mitchell K. Impact of atmospheric surface-layer parameterizations in the new land-surface scheme of the NCEP mesoscale Eta model. Bound-Layer Meteor, 1997, 85: 391–421

33   Louis J F. A parametric model of vertical eddy fluxes in the atmosphere. Bound-Layer Meteor, 1979, 17: 187–202

34   Long P J. Derivation and Suggested Method of Application of Simplified Relations for Surface Fluxes in the Medium-Range Forecast Model: Unstable Case. Office Note 356, US Department of Commerce, National Oceanic and Atmospheric Administration, National Weather Service, National Meteorological Center, 1990, 53

35   Long P J. An Economical and Compatible Scheme for Parameterizing the Stable Surface Layer in the Medium-Range Forecast Model. Office Note 321, US Department of Commerce, National Oceanic and Atmospheric Administration, National Weather Service, National Meteorological Center, 1986. 24

36   Mellor G L, Yamada T. Development of a turbulence closure model for geophysical fluid problems. Rev Geophys, 1982, 20: 851–875

37   Paulson C. The mathematical representation of wind speed and temperature profiles in the unstable atmospheric surface layer. J Appl Meteorol, 1970, 9: 857–861

38   Beljaars A C M, Viterbo P. The sensitivity of winter evaporation to the formulation of aerodynamic resistance in the ECMWF model. Bound-Layer Meteor, 1994, 71: 135–149

39   Yang K, Watanabe T, Koike T, et al. Auto-calibration system developed to assimilate AMSR-E data into a land surface model for estimating soil moisture and the surface energy Budget. J Meteorol Soc Jpn, 2007, 85: 229–242

40   Zilitinkevich S. Non-local turbulent transport: Pollution dispersion aspects of coherent structure of convective flows. Air Poll III, 1995, 1: 53–60

41   Yang K, Ma Y, Koike T, et al. Turbulent flux transfer over bare-soil surfaces: Characteristics and parameterization. J Appl Meteorol Climatol, 2008, 47: 276–290

42   Smith S R, Hughes P J, Bourassa M A. A comparison of nine monthly air-sea flux products. Int J Climatol, 2011, 31: 1002–1027

43   Duan A, Wu G. Weakening trend in the atmospheric heat source over the Tibetan Plateau during recent decades. Part I: Observations. J Clim, 2008, 21: 3149–3164

44   Yanai M, Li C. Mechanism of heating and the boundary layer over the Tibetan Plateau. Mon Weather Rev, 1994, 122: 305–323